Controlling interlayer exchange coupling in one-dimensional Fe/Pt multilayered nanowire

Puspamitra Panigrahi and Ranjit Pati*
Department of Physics, Michigan Technological University, Houghton, Michigan 49931, USA
(Received 13 October 2008; revised manuscript received 10 December 2008; published 8 January 2009)

We report a first-principles density-functional study of interlayer exchange coupling (IEC) in one-dimensional Fe/Pt multilayered nanowire. The magnetic moment of the interfacial Fe atom in the Fe/Pt multilayered nanowire is found to be higher than that of the Fe atom away from the interface. A mechanism based on *multistep electron transfer* between the layers and *spin flip* within the layer is proposed to explain the magnetic-moment enhancement at the interface. The calculated IEC and magnetoresistance are found to switch signs as the width of the nonmagnetic Pt spacer varies. Depending on the width of the Pt spacer, the competition among short- and long-range direct exchanges, indirect Ruderman-Kittel-Kasuya-Yosida exchange, and superexchange is found to be responsible for the nonmonotonous feature in IEC.

DOI: 10.1103/PhysRevB.79.014411 PACS number(s): 75.70.Cn, 71.15.Mb, 73.22.−f, 73.20.−r

I. INTRODUCTION

The discovery of the antiferromagnetic (AFM) coupling between Fe layers across the Cr interlayer of suitable thickness in Fe/Cr multilayered structure[1,2] has spawned considerable interest in the tunable magnetic properties of magnetic/nonmagnetic heterostructures. Subsequent to this pioneering effort, the realization of the phenomenal giant magnetoresistance (GMR) effect up to 80% in the antiferromagnetically coupled Fe/Cr, Co/Cu, and Fe/Cu multilayered structures[3,4] has fueled further interest in heterostructures. In contrast to the previously observed monotonically decreasing trend of GMR (Refs. 3 and 4) and hence the interlayer exchange coupling (IEC) with spacer layer thickness, successive studies have reported both long (10–15 Å) and short (3–4 Å) period oscillations.[5–7] Similar oscillations of IEC have also been found even when transition metals including Pt and noble metals such as Cu and Au are used as spacers in multilayered structures.

Among the various theories put forward, the model based on the Ruderman-Kittel-Kasuya-Yosida (RKKY) theory has been able to give a very clear explanation of the observed oscillations in IEC. Based on the RKKY model and taking surface roughness, geometry, and thickness of spacer layer into account, a lucid explanation[8,9] is given for the long and multiperiodic oscillations of IEC. It should be noted that the other model based on quantum well states[10,11] has also been successful in explaining the observed oscillatory magnetic coupling. However, all these qualitative explanations do not satisfactorily elucidate the quantitative predictions such as strength of the exchange coupling J which significantly depends on the degree of matching of energy bands at the magnetic/nonmagnetic interface. The *ab initio* density-functional calculations based on local spin-density approximations[12–15] are able to provide the value of J with precision. The calculated energy difference between the AFM and ferromagnetic (FM) couplings, which represents the strength of the interlayer coupling energy $J=E_{(d)}^{\uparrow\downarrow}-E_{(d)}^{\uparrow\uparrow}$, is found to exhibit a slowly decaying oscillation with spacer layer thickness, in good agreement with experimental results.[16–18] These seminal works have contributed to the development of GMR-based read head sensor, which is used presently in high-density hard drive disk.

Current demand for ultrahigh-density and high sensitive memory devices has incited researchers to search for novel low-dimensional multilayered materials. In fact, currently the multilayered nanowires have been found to exhibit GMR effect at ambient temperature.[19–21] Dependence of GMR on spacer width is also observed in multilayered nanowire system.[22] Furthermore, massive fabrication of freestanding one-dimensional (1D) multilayered nanowires with complete control over magnetic and nonmagnetic layer sequences has been reported.[23,24] Though we have started to witness a surge in theoretical interest toward metallic nanowires[25–27] and tunnel junctions[28] in recent years, only limited calculations have been reported in multilayered nanowires to understand the crucial atomic scale structural heterogeneity at the magnetic/nonmagnetic interface and its role on IEC.

In the present paper we have used Fe/Pt multilayered nanowire systems and *ab initio* density-functional theory to reveal the role of spacer width in controlling the J value. The interest in Fe/Pt system is prompted by their multifaceted physical properties. For example, in the absence of external magnetic field the Fe/Pt system acts as a permanent magnet. Invar effect as well as magnetostriction effect has also been observed in Fe/Pt systems.[29,30] Furthermore, fabrication of Fe/Pt nanowire has been reported.[31,32] The influence of size and shape of nanowire on magnetic domain pattern in 1D Fe nanowire has also been revealed very recently.[33] In our previous work, the role of Pt spacer in tuning the FM property of Fe/Pt nanowire is addressed.[34] The average magnetic moment per Fe atom is found to increase with the increase in Pt spacer width and has been shown to follow an $\sim 1/N_{\mathrm{Fe}}$ trend; N_{Fe} is the number of Fe layers in the Fe/Pt nanowires. But, the AFM coupling between the Fe layers on the opposite sides of the Pt spacer is not considered. Here, we have considered both FM and AFM couplings between the Fe layers for different Pt spacer widths. The local spin-density-functional calculation is performed using VASP code.[35] We have found that the magnetic moment of iron atom increases at the interface due to competition between the spin flip within a layer and the multistep electron transfer between the layers depending on the spacer layer thickness. Furthermore, the J value is found to switch signs as we go from two to five Pt spacer layers. Increasing the number of spacer layer from five to eight, switching of the sign of J value is again ob-

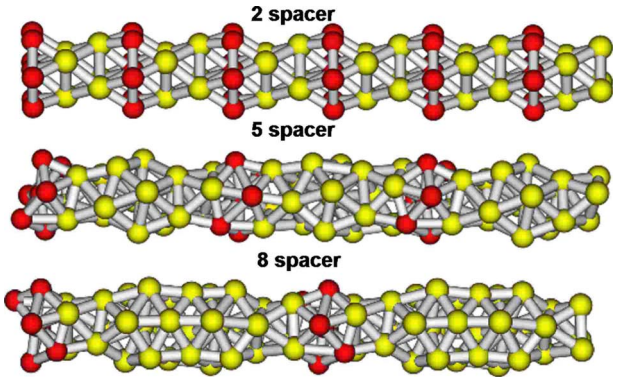

FIG. 1. (Color online) Optimized structures for the Fe/Pt nanowire with two Pt spacer, five Pt spacer, and eight Pt spacer layers. Notations: dark gray (red), Fe; light gray (yellow), Pt.

served but the magnitude of J is found to be significantly smaller. This clearly explains the role of spacer layer thickness in modulating the magnetic moment as well as IEC—an important requirement for their potential application in magnetoelectronics. Competition among short-range and long-range direct exchanges, indirect RKKY exchange, and superexchange is invoked to explain the switching of the sign of J with the increase in spacer width.

The rest of the paper is organized as follows. In Sec. II, a brief description of theoretical approach is provided. Section III discusses results and Sec. IV summarizes our main results.

II. THEORETICAL APPROACH

As the atomic level structural details are not available *a priori* for the proposed magnetic nanowires and structure determination from the scratch poses a formidable challenge, we have used the bulk experimental structure as the guiding point for constructing the nanowire structure as described in our previous study.[34] Both Fe and Pt have fcc bulk structures. From the atomic arrangements in the fcc bulk structure, the nanowire is constructed along the (111) direction whose unit cell repeats in every three planes (*ABCABC*). For two layers of Pt spacer (Fig. 1), a unit cell of 26 atoms from the (*ABCABCABC*…) periodic series is engineered in the form of a tetragonal lattice with a lattice parameter of 12.12 Å. The other two sides of the unit cell are taken as 15 Å to ensure negligible interaction of the nanowire with its image in the x and the y directions. From this *ABCABC* periodic series, A layer accommodates seven Fe atoms; B and C layers have three Pt atoms each. To achieve the ferromagnetic coupling, the spins of two A layers are kept in parallel configuration with each other. For the AFM coupling, their spins are kept at antiparallel alignment. We have used first-principles density-functional approach[36] with local spin-density approximation for exchange and correlation in our calculation. The optimized structures in the FM and AFM configurations are obtained using the stringent force criterion of 0.01 eV/Å for the individual atom. During the self-consistent calculation the convergence criterion for energy is taken to be 10^{-6} eV. We have used plane-wave basis set and ultrasoft pseudopotential (USPP) for our calculations. The interlayer exchange coupling (J) is calculated from the difference in total energy between the FM and AFM configurations as $J=\frac{E_{(d)}^{\uparrow\uparrow}-E_{(d)}^{\uparrow\downarrow}}{n}$, where n is the number of atoms in the unit cell. In a representative nanowire with two Pt spacer layers in the unit cell, we have also used the projected augmented wave (PAW) potential[35] to test the validity of the results for J with respect to the choice of the potential. It is found that the use of PAW potential with $(1\times1\times1)$ k-point sampling within the Monkhorst-Pack (MP) scheme for structure optimization gives a J value of 19.6 meV as compared to 15.4 meV from USPP with the same k-point sampling of the Brillouin zone (BZ). Though the use of PAW potential yields a higher J value, the sign of the J value, which is of interest to us, remains unchanged. The sensitiveness of the J is also tested by optimizing the structure for two Pt spacer nanowires using $(1\times1\times3)$, $(1\times1\times5)$, and $(1\times1\times7)$ k-point samplings of the BZ within the MP scheme. Use of $(1\times1\times3)$ k-point sampling of the BZ during structural optimization gives the J value of 9.6 meV, which changes to 9.5 and 9.3 meV for $1\times1\times5$ and $1\times1\times7$ k-point samplings, respectively. The relative difference in J value between $1\times1\times5$ and $1\times1\times7$ is only 2%. It is also important to note that the sign of the J value remains unchanged with respect to the choice of k-point sampling. Considering the spin-polarized nature of the problem and relatively larger size of the unit cell and the excellent convergence in J value in two Pt spacer nanowire, we have used $1\times1\times5$ k-point sampling of the BZ during geometry optimization for the five and eight spacer layer nanowires. For five spacer layers (Fig. 1), the first and the third A layers are chosen to be the magnetic Fe layers whereas the *BCABC* layers in between are chosen as the nonmagnetic Pt layers. In the case of eight spacer layers (Fig. 1), the first and the tenth A layers are the magnetic Fe layers whereas the *BCABCABC* layers in between are the nonmagnetic Pt layers. The spins in the magnetic layers are aligned in parallel and antiparallel configurations to obtain the FM and AFM couplings between the magnetic layers. Similar procedures as discussed above for two spacer layers are used to obtain the IEC as a function of the spacer length.

We have used $1\times1\times5$ k-point mesh for calculating the electronic band structure and magnetic moments. A large plane-wave cutoff of 237.6 eV is taken to include reasonably large number of plane waves in the basis set and kept fixed for all subsequent calculations. To calculate the local magnetic moment of individual atom, the Wigner-Seitz radii for Fe and Pt are taken as 2.46 and 2.75 a.u., respectively.

III. RESULTS AND DISCUSSIONS

The optimized nanowire structures for different spacer lengths are depicted in Fig. 1. In the case of two spacer layers, only a minor relaxation from the *ABCABC* packing of the fcc structure is noted for both FM and AFM configurations. It should be noted that in the AFM configuration, the atomic level structural relaxations due to spin flips are explicitly included in our calculations. Increasing the Pt spacer width, a significant distortion from the *ABCABC* packing of

TABLE I. Comparison of individual magnetic moments (unit μ_B) of Fe atom in the two-spacer, five-spacer, and eight-spacer layer multilayered nanowire systems in both FM and AFM configurations with that of corresponding Fe atoms in pristine Fe nanowires.

		Two-spacer layer (α-β)		Five-spacer layer (α-β)		Eight-spacer layer (α-β)	
Atoms	Pristine	Ferromagnetic	Antiferromagnetic	Ferromagnetic	Antiferromagnetic	Ferromagnetic	Antiferromagnetic
Fe1	0.990	2.257	1.877	2.231	2.137	2.197	2.196
Fe2	2.746	3.085	2.911	3.175	3.165	3.088	3.088
Fe3	2.743	3.085	2.911	2.997	3.090	3.088	3.089
Fe4	2.746	3.107	3.037	3.054	3.067	3.087	3.089
Fe5	2.743	3.107	3.037	2.725	3.074	3.065	3.064
Fe6	2.743	3.108	3.037	2.725	3.056	3.065	3.063
Fe7	2.745	3.108	3.037	2.720	3.012	3.087	3.088

the fcc is evident due to a strong buckling in the *A* plane. A similar structural configuration is obtained for the AFM configuration. Analysis of individual magnetic moments in the FM and AFM configurations reveals an increase in Fe magnetic moment at the Fe/Pt interfacial site compared to the Fe atom far away from the interface. It should be noted that the magnetic moment of Fe far away from the interface is almost the same as that obtained in the pristine Fe nanowire. A similar increase in magnetic moment at the interfacial Fe atoms is also observed in our previous study.[34] Furthermore, in Fe/Pt bulk structure,[37] magnetic-moment enhancement for the interfacial Fe atom is also reported. To understand the cause of this increase in magnetic moments of Fe atom at the interface, the magnetic moments of the individual Fe atoms at the most affected interfacial *A* layer from the *ABCABC* series are summarized in Table I.

A substantial change in magnetic moment for the core Fe atom is noted between pristine and multilayered nanowires (Table I). Magnetic moment arises from the imbalance between spin-up (α) and spin-down (β) populations. Thus, to understand this increase in magnetic moment, α and β populations of Fe atoms in layer *A* are compared with the corresponding spin populations in pristine Fe nanowires. In the case of two Pt spacers, as illustrated in Fig. 2, for the FM configuration, an increase in α population and decrease in β population are found for the Fe atom in the *A* layer. It should be noted that the increase in α population is not the same as the decrease in β population, suggesting spin flip is not the only reason for magnetic-moment enhancement at the interface. Analyzing the α and β populations of the nearby spin-polarized Pt atom, we found that the increase in α population for Fe in *A* layer is due to the transfer of α electron from the nearest Pt layer; the decrease in β population is due to the transfer of β electron from Fe atoms in the *A* layer to the interfacial Pt atoms in the *B* layer (step I in Fig. 2). As a result the difference between α and β populations of interfacial Fe layers widens, resulting in an increase in their magnetic moment μ. This electron transfer process would, in fact, lead to a negative μ at the interfacial Pt atom. However, our analysis reveals small positive μ at the interfacial Pt atoms. This could be understood from the fact that the presence of a strong magnet in the vicinity of the magnetically polarized Pt atoms realigns the small magnetic moment of the Pt to the direction of that in Fe through spin flip (step II in Fig. 2). A similar mechanism is found to be valid for the AFM configuration. But the magnitude of μ at Fe is found to be higher in the FM case as compared to the AFM configuration.

In the case of five spacer layers in the unit cell, analogous *spin transfer and spin-flip* effects are also observed. The Pt layer near the Fe/Pt interface has positive μ, which decreases monotonically with the increase in the number of spacer layers from the interface and becomes negative for the Pt layer far away from the interface. Thus the electron transfer process here can be viewed as a *multistep spin transfer* process. In an eight-spacer layer system, the observed enhancement of magnetic moment of interfacial Fe atoms can be attributed to the same reason.

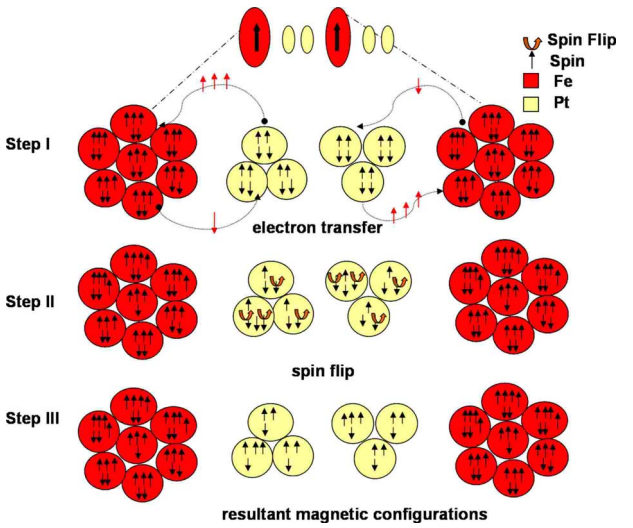

FIG. 2. (Color online) Schematic representation of *spin-flip and electron transfer mechanisms* in the nanowire with two Pt spacer in the unit cell. Step I—*ABCABC* unit cell of the nanowire with two Pt spacer (*BC*) layers in between two Fe(*A*) layers in their respective spin configurations prior to the interaction between Fe and Pt. Two *A* layers are in the parallel spin configuration. Curved paths indicate the spin transfer process between the layers after the interaction between Fe and Pt is taken into account. Step II—the resultant spin configuration after the spin transfer process between the layers. Curved arrows indicate the spin-flip process within the layer. Step III—resultant magnetic configurations of the Fe/Pt nanowire after the spin-flip and electron transfer processes.

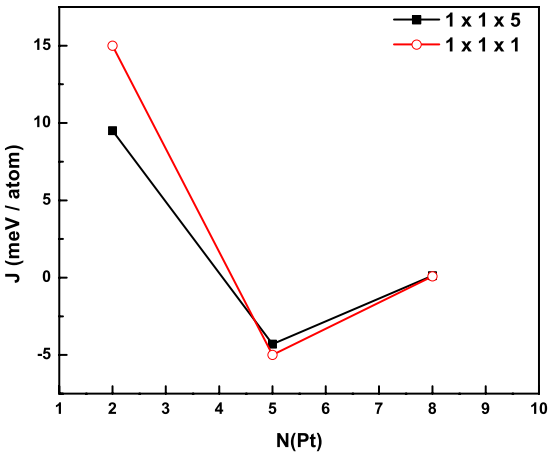

FIG. 3. (Color online) Calculated interlayer exchange coupling (J) as a function of number of nonmagnetic Pt spacer layers N(Pt) in the nanowire structures. $1\times1\times1$ and $1\times1\times5$ represent the k-point sampling of the BZ used to obtain the respective results.

The calculated IEC as a function of spacer layer thickness is summarized in Fig. 3. One can note from Fig. 3 that the magnitude of J value decreases with the increase in spacer width. Both $1\times1\times1$ and $1\times1\times5$ k-point samplings of the BZ yield similar trend in IEC. For the eight-Pt-spacer layer in the unit cell, the J value is found to be substantially smaller. But the most interesting result in Fig. 3 is the switching of the sign of J. Increasing the number of Pt spacer layers from two to five, the J value is found to change signs (becoming negative). The AFM configuration is stable for two-spacer layer system. The FM configuration is found to be more stable for five-spacer layer. Increasing the number of spacer layer from five to eight, switching of the sign of J value is again observed, suggesting the stability of the AFM configuration over the FM ordering. In bulk multilayered system, similar switching in J value with the increase in spacer width is also observed[5–7] and has been explained by invoking RKKY model. It is important to note that, very recently, Brovko *et al.*[38] showed a similar oscillation in the exchange coupling between two magnetic adatoms by varying the size of the atomic spacer chain.

To understand the origin of switching in J value in the nanowire, we analyzed the magnetic moment per atom layerwise. The results are summarized in Fig. 4. One can notice from Fig. 4(a) that for two-Pt-spacer system, because of the strong overlap between the interlayer Pt wave functions, Pauli's exclusion principle requires the spins in Pt layer to be in antiparallel alignment. Thus the negative direct exchange interaction is favored over the positive direct exchange interaction (parallel spin alignment) between Pt layers. These magnetic arrangements in Pt layers favor indirect RKKY-type exchange interaction between the Fe layers resulting in a stable AFM coupling. In the case of five-Pt-spacer system [Fig. 4(b)], the distance between spin-polarized Pt layers (2 and 5; 2 and 6; 3 and 5; and 3 and 6) increases, favoring the positive direct exchange interaction over the negative direct exchange. Thus the FM coupling between Fe layers is favored over the AFM coupling. The magnitude of magnetic moment per atom in the fourth Pt layer is substantially smaller to initiate the negative direct exchange interaction between the Pt atoms within the layer as seen for the two-Pt spacer. One could also use indirect RKKY exchange interaction of a different period to explain the stability of the FM coupling in the case of five-layer Pt spacer. It is also noteworthy to point out that the small asymmetry in the magnitude of average magnetic moment between the Fe-A layers shown in Fig. 4(b) is due to small local structural asymmetry around the A layer in the optimized structure. In the case of eight Pt spacer layers in the unit cell of the wire, as the distance between Fe layers increases, the superexchange interaction plays the dominant role in favoring the AFM coupling over the FM coupling between the Fe layers. Layers 4–7, as shown in Fig. 4(c), have almost zero magnetic moment per atom. These Pt atoms are covalently bonded, resulting in the stability of the AFM coupling mediated by these nonmagnetic Pt spacer atoms.

To develop an atomic level understanding of the switching of J and its role in the electronic properties of the nanowire, the spin-polarized energy bands are calculated for the three nanowires. The results obtained using $1\times1\times5$ k-point sampling of the BZ are summarized in Fig. 5. In the case of two spacer layers in the unit cell, for the FM configuration [Fig. 5(a)], the α valence band and conduction band near the Fermi energy show a clear Fe(s,p,d) with Pt(s,p,d) hybridization; the β valence band is mostly Fe(d) and Pt(d) hybrid band, and β conduction band shows a dominant Fe(d) character. In the case of the stable AFM configuration, both the valence band and conduction band near the Fermi energy are mostly Fe(d,p) and Pt(d,p) hybrid bands. Thus the strong d-p hybridization favors the AFM coupling over the FM coupling in the case of two Pt spacer layers in the unit cell. Similar d-p hybridization favoring the AFM configuration over the FM configuration was reported in NiAl nanowire.[39]

For the five-spacer-layer nanowire in the FM (stable) configuration, both spin-up valence and conduction bands near the Fermi energy [Fig. 5(b)] are found to have Pt(d) character. But as we move away from the high-symmetry point the bands develop Fe/Pt(d,p) hybrid character contributing to the stability of the FM configuration. In the spin-down case both valence and conduction bands are Fe(d) and Pt(d) hybrid bands with dominant Fe(d) character at the high-symmetry point. In the case of the AFM configuration both valence and conduction bands are primarily Pt(d) bands. Thus the weakening of the Fe-Pt hybridization in the AFM configuration case results in an unstable AFM ordering. In the case of eight Pt spacer layers in the unit cell, the valence and conduction bands near the Fermi energy are mostly Pt(d) bands with very little Fe(d) character. Here bonding between Pt atoms is mostly covalent in nature. Thus the strong covalency within the Pt layer favors the AFM coupling between Fe via the superexchange interaction.

To further understand the J switching and its implication on magnetoresistance for practical applications, we have calculated the polarization, conductance, and magnetoresistance for different spacer lengths. These results obtained using $1\times1\times5$ k-point sampling of the BZ are summarized in Table II. From Table II, one can notice switching of the sign of the polarization at the Fermi energy between two and five spacer systems. Increasing from five to eight spacer layers in the

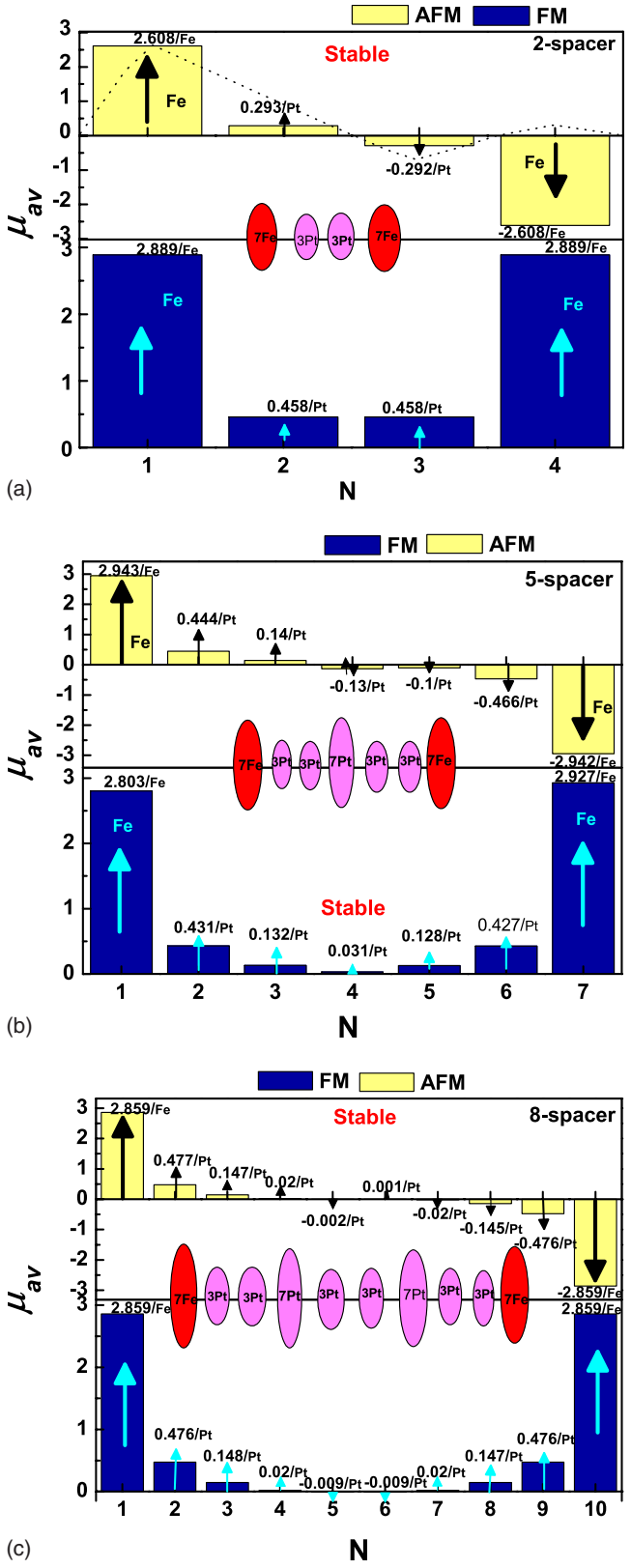

FIG. 4. (Color online) Histogram plot for the average magnetic moment per atom (μ_{av}) in FM and AFM configurations. (a) Two Pt spacer; (b) five Pt spacer; and (c) eight Pt spacer nanowires. Notations: dark gray (blue), FM; light gray (yellow), AFM; **N** is the layer number; dotted line in (a) represents RKKY type magnetic perturbation.

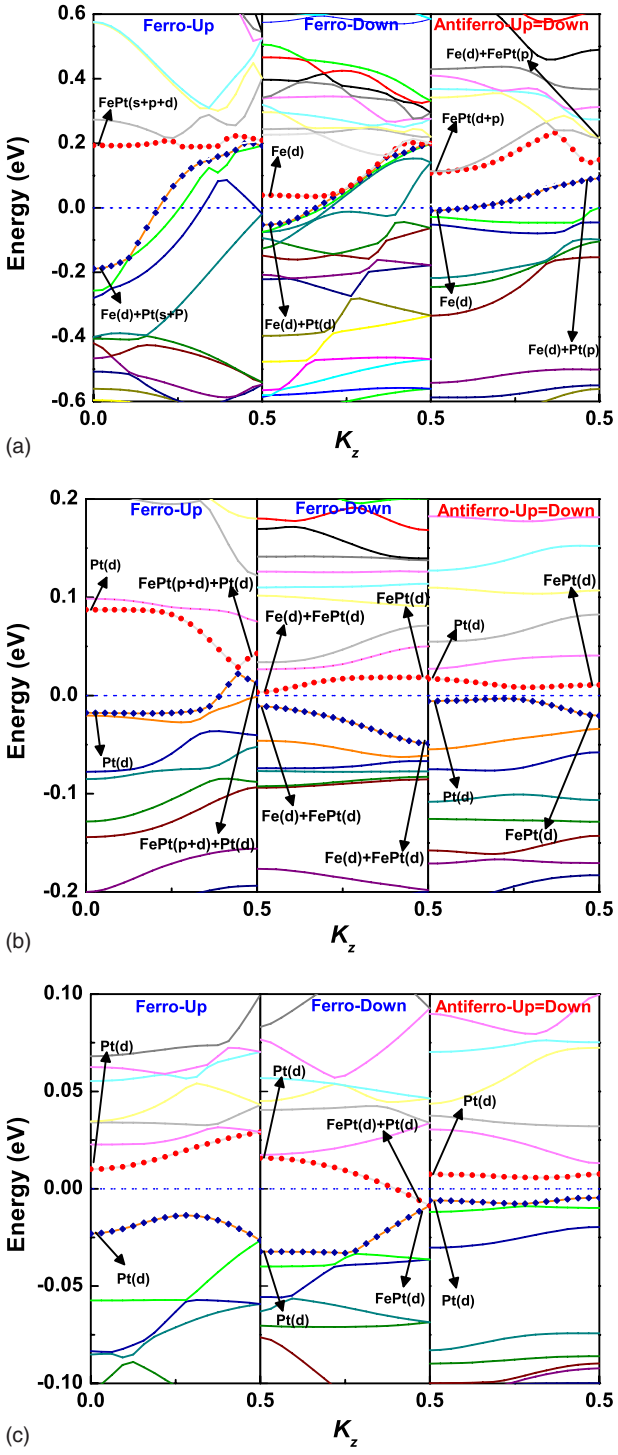

FIG. 5. (Color online) Spin-polarized energy-band structures: (a) two-spacer; (b) five-spacer; (c) eight-spacer layer nanowires. The Fermi energy is set at $E=0$. Notations: gray (red) circle, conduction band; gray (blue) diamond, valence band.

unit cell, the polarization at the Fermi energy again changes sign. This polarization switching is expected to affect the magnetoconductance of the wire. Thus, we invoke the simple Julliere's model[40] to calculate the conductance in the FM and AFM configurations. GMR value is calculated from the conductances G_{FM} and G_{AFM}. The GMR value obtained for dif-

TABLE II. Calculated polarization, conductance, and GMR in the nanowire for different spacer lengths.

	Two spacer		Five spacer		Eight spacer	
	FM	AFM	FM	AFM	FM	AFM
Polarization (p) [a]	−0.9192	0	0.3385	0	−0.3	0
Conductance (G) [b]	1.2713	0.544	0.898	1.125	0.7848	0.58
GMR[c]	57%		−27%		26%	

[a]Polarization $(p)=\frac{\mathrm{DOS}_{E_F}(\alpha)-\mathrm{DOS}_{E_F}(\beta)}{\mathrm{DOS}_{E_F}(\alpha)+\mathrm{DOS}_{E_F}(\beta)}$; $\mathrm{DOS}_{E_F}(\alpha)$ corresponds to the spin-up (α) density of states at the Fermi energy and $\mathrm{DOS}_{E_F}(\beta)$ corresponds to the spin-down (β) density of states at the Fermi energy.
[b]Conductance in the FM case, $G_{\mathrm{FM}}=[\mathrm{DOS}_{E_F}(\alpha)]^2+[\mathrm{DOS}_{E_F}(\beta)]^2$; for the AFM configuration, $G_{\mathrm{AFM}}=2\mathrm{DOS}_{E_F}(\alpha)\mathrm{DOS}_{E_F}(\beta)=2[\mathrm{DOS}_{E_F}(\alpha)]^2$, obtained using simple Jullier's model (Ref. 40).
[c]$\mathrm{GMR}=\frac{G_{\mathrm{FM}}-G_{\mathrm{AFM}}}{G_{\mathrm{FM}}}\times 100\%$.

ferent spacer configurations also shows switching of signs as noted for J.

IV. SUMMARY

In summary, using first-principles density-functional approach, we report a comprehensive study on the role of atomic scale structural heterogeneity at the magnetic/nonmagnetic interface in modulating the IEC in 1D Fe/Pt nanowire. We have found enhancement in the magnetic moment of the Fe at the Fe/Pt interface as compared to the magnetic moment of the Fe atom away from the interface. A mechanism based on *multistep electron transfer and spin flip* is proposed to explain the increased magnetic moment of the interfacial Fe atom. The J value as well as GMR is found to switch signs as the spacer width in the nanowire increases. Magnitude of J value is found to decrease substantially for larger spacer width. The competition among short-range and long-range direct exchanges, indirect exchange, and superexchange depending on the spacer width is found to be responsible for the nonmonotonous sign in J.

*patir@mtu.edu

[1] P. Grünberg, J. Appl. Phys. **57**, 3673 (1985).
[2] P. Grünberg, R. Schreiber, Y. Pang, M. B. Brodsky, and H. Sowers, Phys. Rev. Lett. **57**, 2442 (1986).
[3] M. N. Baibich, J. M. Broto, A. Fert, F. Nguyen Van Dau, F. Petroff, P. Etienne, G. Creuzet, A. Friederich, and J. Chazelas, Phys. Rev. Lett. **61**, 2472 (1988).
[4] G. Binasch, P. Grünberg, F. Saurenbach, and W. Zinn, Phys. Rev. B **39**, 4828 (1989).
[5] S. S. P. Parkin, N. More, and K. P. Roche, Phys. Rev. Lett. **64**, 2304 (1990).
[6] S. S. P. Parkin, R. Bhadra, and K. P. Roche, Phys. Rev. Lett. **66**, 2152 (1991).
[7] S. T. Purcell, W. Folkerts, M. T. Johnson, N. W. E. McGee, K. Jager, J. aan de Stegge, W. B. Zeper, W. Hoving, and P. Grünberg, Phys. Rev. Lett. **67**, 903 (1991).
[8] P. Bruno and C. Chappert, Phys. Rev. Lett. **67**, 1602 (1991).
[9] P. Bruno and C. Chappert, Phys. Rev. B **46**, 261 (1992).
[10] D. M. Edwards, J. Mathon, R. B. Muniz, and M. S. Phan, Phys. Rev. Lett. **67**, 493 (1991).
[11] J. E. Ortega, F. J. Himpsel, G. J. Mankey, and R. F. Willis, J. Appl. Phys. **73**, 5771 (1993).
[12] P. Lang, L. Nordström, R. Zeller, and P. H. Dederichs, Phys. Rev. Lett. **71**, 1927 (1993).
[13] R. Hafner, D. Spišák, R. Lorenz, and J. Hafner, J. Phys.: Condens. Matter **14**, 4297 (2002).
[14] J. Opitz, P. Zahn, J. Binder, and I. Mertig, Phys. Rev. B **63**, 094418 (2001).
[15] J. Kudrnovský, V. Drchal, I. Turek, P. Bruno, and P. Weinberger, J. Phys.: Condens. Matter **13**, 8539 (2001).
[16] A. Yoshihara, J. T. Wang, K. Takanashi, K. Himi, Y. Kawazoe, H. Fujimori, and P. Grünberg, Phys. Rev. B **63**, 100405(R) (2001).
[17] B. Heinrich, Z. Celinski, J. F. Cochran, W. B. Muir, J. Rudd, Q. M. Zhong, A. S. Arrott, K. Myrtle, and J. Kirschner, Phys. Rev. Lett. **64**, 673 (1990).
[18] J. E. Mattson, C. H. Sowers, A. Berger, and S. D. Bader, Phys. Rev. Lett. **68**, 3252 (1992).
[19] A. Blondel, J. P. Meier, B. Doudin, and J.-Ph. Ansermet, Appl. Phys. Lett. **65**, 3019 (1994).
[20] L. Piraux, J. M. George, J. F. Despres, C. Leroy, E. Ferain, R. Legras, K. Ounadjela, and A. Fert, Appl. Phys. Lett. **65**, 2484 (1994).
[21] M. Tanase, D. M. Silevitch, A. Hultgren, L. A. Bauer, P. C. Searson, G. J. Meyer, and D. H. Reich, J. Appl. Phys. **91**, 8549 (2002).
[22] J. A. Katine, A. Palanisami, and R. A. Buhrman, Appl. Phys. Lett. **74**, 1883 (1999).
[23] J. Choi, S. J. Oh, H. Ju, and J. Cheon, Nano Lett. **5**, 2179 (2005).
[24] Y. Peng, T. Cullis, G. Mobus, X. Xu, and B. Inkson, Nanotechnology **18**, 485704 (2007).
[25] A. Delin, E. Tosatti, and R. Weht, Phys. Rev. Lett. **92**, 057201 (2004).

[26] B. Yu. Yavorsky and I. Mertig, Phys. Rev. B **74**, 174402 (2006).
[27] J. C. Tung and G. Y. Guo, Phys. Rev. B **76**, 094413 (2007).
[28] K. M. Smelova, D. I. Bazhanov, V. S. Stepanyuk, W. Hergert, A. M. Saletsky, and P. Bruno, Phys. Rev. B **77**, 033408 (2008).
[29] S. Khmelevskyi, A. V. Ruban, Y. Kakehashi, P. Mohn, and B. Johansson, Phys. Rev. B **72**, 064510 (2005).
[30] S. Khmelevskyi and P. Mohn, Phys. Rev. B **69**, 140404 (2004).
[31] Y. Hou, H. Kondoh, R. Che, M. Takeguchi, and T. Ohta, Small **2**, 235 (2006).
[32] J. Gao, Q. Zhan, W. He, D. Sun, and Z. Cheng, Appl. Phys. Lett. **86**, 232506 (2005).
[33] S. Shiraki, H. Fujisawa, T. Nakamura, T. Muro, M. Nantoh, and M. Kawai, Phys. Rev. B **78**, 115428 (2008).
[34] P. Panigrahi and R. Pati, Phys. Rev. B **76**, 024431 (2007).
[35] Vienna ab initio Simulation Package, Technische Universität Wien, 1999; G. Kresse and J. Furthmüller, Phys. Rev. B **54**, 11169 (1996).
[36] R. G. Parr and W. Yang, *Density-Functional Theory of Atoms and Molecules* (Oxford University Press, New York, 1989).
[37] M. Podgorny, Phys. Rev. B **43**, 11300 (1991).
[38] O. O. Brovko, P. A. Ignatiev, V. S. Stepanyuk, and P. Bruno, Phys. Rev. Lett. **101**, 036809 (2008).
[39] P. P. Pal and R. Pati, Phys. Rev. B **77**, 144430 (2008).
[40] M. Julliere, Phys. Lett. **54A**, 225 (1975).